Current Biology, Volume *23*

Supplemental Information

Asynchronous Broadband Signals Are the Principal Source of the BOLD Response in Human Visual Cortex

Jonathan Winawer, Kendrick N. Kay, Brett L. Foster, Andreas M. Rauschecker, Josef Parvizi, and Brian A. Wandell

Supplemental Inventory

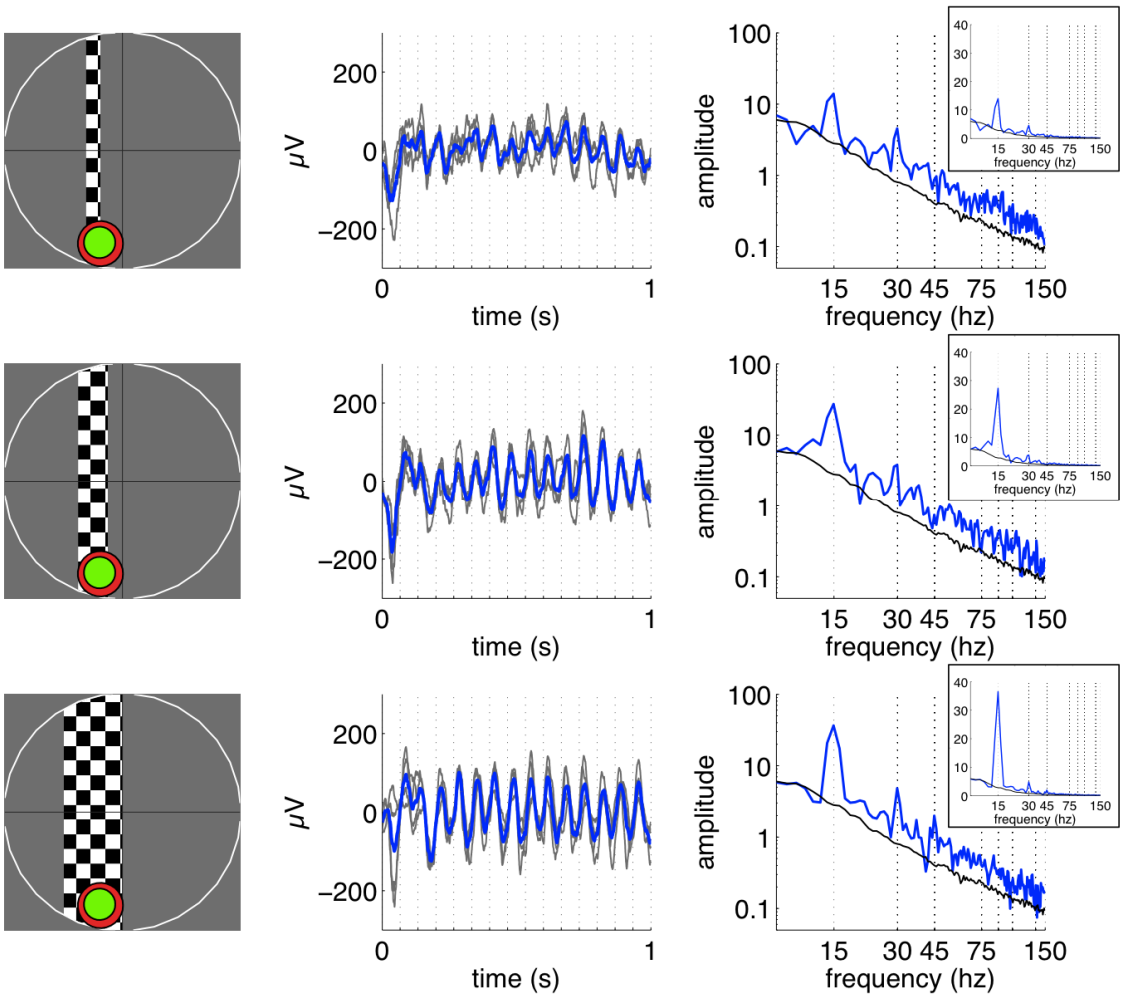

Figure S1. Example Responses to Bars of Different Widths

The left column shows the stimulus during one portion of the moving bar experiment. The discs indicate the 2-sigma extents of the Gaussian receptive fields estimated from the broadband (red) or stimulus-locked (green) responses. The middle column shows the voltage time series during the 1-s windows that the bar was in this position. The gray traces are the 4 individual trials (2 experiments with each bar width * 2 passes through this location per experiment) and the blue traces are the mean. The amplitudes of the periodic fluctuation are largest for the wide bar and smallest for the narrow bar. The dotted vertical lines denote checkerboard contrast reversal times. The right column shows the amplitude spectrum during the same 1 s window. The blue trace is the mean of the spectra computed from each of the four time series, and the black is the mean response during stimulus blanks. The three stimuli evoke a similar broadband elevation in the spectra, whereas the stimulus-locked response (peak at 15 Hz) increases with bar width. Insets show the same data on a linear amplitude scale. The stimulus-locked response increase to bar width is more salient on the linear scale and the broadband response is more visible on the log scale. Data are from the same electrode depicted in Figure 1.

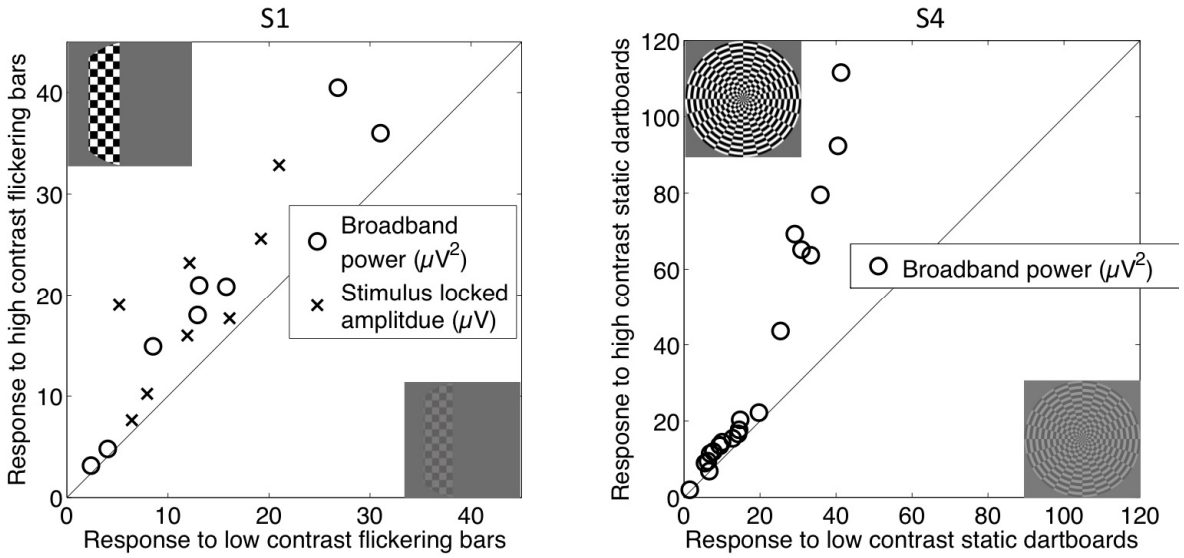

Figure S2. The ECoG Broadband Response Is Sensitive to the Level of Luminance Contrast in the Stimulus

(Left) Moving bar experiments were conducted for subject S1 at multiple contrast levels. For each of 8 visually responsive channels in V1, V2 and V3 for S1, the peak broadband and peak stimulus locked response were extracted for each of the 8 bar sweeps across the screen, for each contrast level (8 peaks per contrast level per electrode). The mean of the 8 peaks is plotted for a 10% contrast stimulus (x-axis) and 78% contrast stimulus (y-axis). The 10% contrast level was used for fitting the pRF models for S1. An example of the high contrast stimulus and the low contrast stimulus are shown in the upper left and lower right, respectively. Both the broadband power (circles, μV^2) and stimulus-locked amplitude (x's, μV) are elevated for the high contrast stimulus.

(Right) Static, large-field dartboard patterns of various contrast levels were shown to subject S4. The broadband response power for two contrast levels (90% versus 8%) is plotted for visually responsive electrodes in V1/V2/V3. In all channels, response power increases with contrast. Contrast of 8% was used for the moving bar experiments for S4. The fact that, in both subjects, broadband response increases with stimulus contrast indicates that the response saturation in the broadband signal observed with increasing stimulus size (Figure 2) is not likely due to a response ceiling effect.

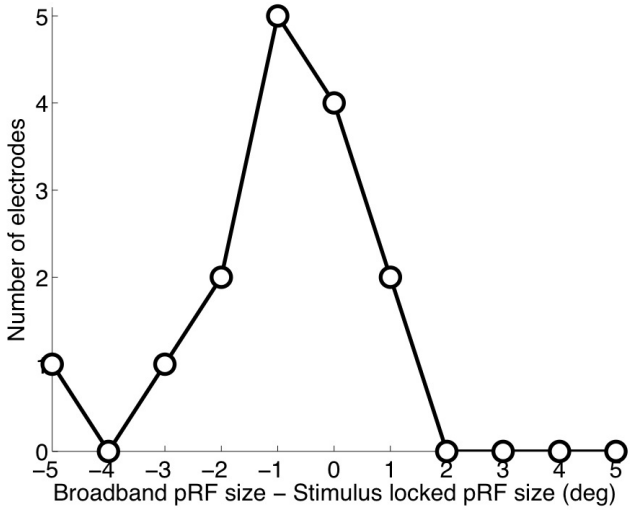

Figure S3. Population Receptive Field Size Measured from the Broadband and Stimulus-Locked Signals

The histogram plots the difference between the pRF size (defined in equation 1 as [sigma of the Gaussian] / sqrt[standard deviation of the exponent]). Values to the right of 0 indicate a larger pRF size measured in the broadband signal and values to the left of 0 indicate a larger pRF size measured in the stimulus locked signal. The pRF size and exponent for each of the visually responsive electrodes in V1, V2, and V3 in subjects S1-S3 are reported in Table S1. The pRF centers estimated by the two signal components are plotted in Figure 3.

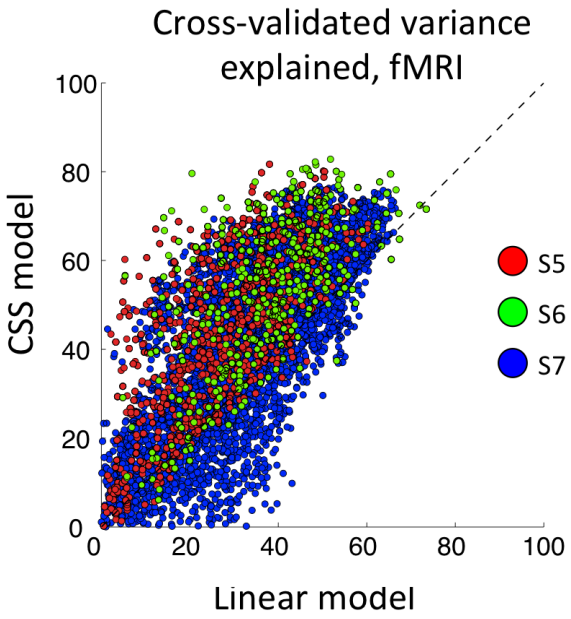

Figure S4. Accuracy of CSS Model and Linear Model for fMRI Data

Functional MRI data from 3 subjects were fit to the CSS model and a linear model (S5, S6, S7; red, green and blue dots). Accuracy was assessed by cross-validation. For each subject, scans were conducted with 3 different bar widths. The models were fit to data from scans with two bar widths and tested against data from the left-out scan with the third bar width. Plots show the variance explained for the left-out data, with each point corresponding to one voxel. Voxels come from V1, V2 or V3, and were selected based on a linear fit to bar scans containing only the largest bar width at high contrast (>30% variance explained). In two of three subjects (S5, S6), nearly every voxel was more accurately fit by the CSS model than the linear model (data points above the identity line). For S7, the majority of voxels were better fit by the CSS model, though at low variance explained, some voxels were better fit by the linear model. The pattern observed here is similar to the pattern in the broadband ECoG signal (Figure 4).

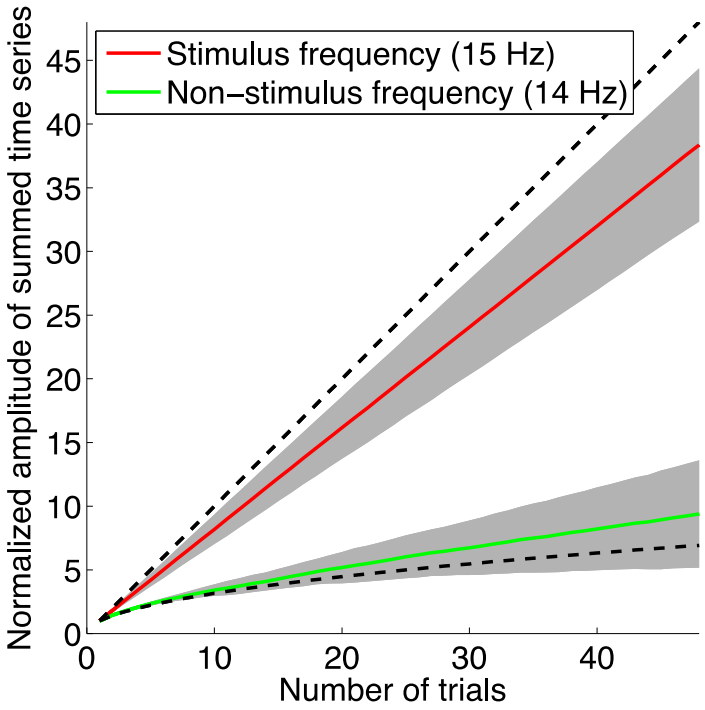

Figure S5. Response Amplitude to Large-Field On-Off Flicker Summed over Trials

The amplitudes of the responses at the stimulus frequency (15 Hz) and a non-stimulus frequency (14 Hz) were computed for time series summed across 1-second data chunks with large-field periodic stimulation in each of 16 channels. For each channel, the 48 chunks (trials) were randomly reordered 1000 times, and a cumulative sum was computed across the re-ordered trials. The amplitude at a given frequency (e.g., 15 Hz) was averaged across the 1,000 sequences at each trial number (1 to 48), yielding one curve per channel per frequency. These curves were averaged across 15 channels for the stimulus frequency (15 Hz) and a non-stimulus frequency (14 Hz). The amplitude of the stimulus frequency (red) grows close to linearly with the number of trials, whereas the amplitude at a different frequency (green) grows approximately with the square root of the number of trials. Shading indicates +/-1 standard deviation across 15 channels. The linear and square root predictions are shown with dashed lines, extrapolated from the mean amplitude for a single trial. The plot indicates that for the stimulus-locked response, additivity approximately holds in the amplitude domain. In contrast, the phase of the non-stimulus-locked responses is random; because the amplitude at the non-stimulus frequency grows with the square root of the number of trials, power (not amplitude) will be additive across trials. A consequence of this is that when analyzing data from multiple trials, the coherent transform (averaging in the time domain and then computing the amplitude of the Fourier transform) and the coherent transform (computing the transform on each trial and averaging the coefficients) yields similar values at the stimulus frequency, but not other frequencies (Figure 5).

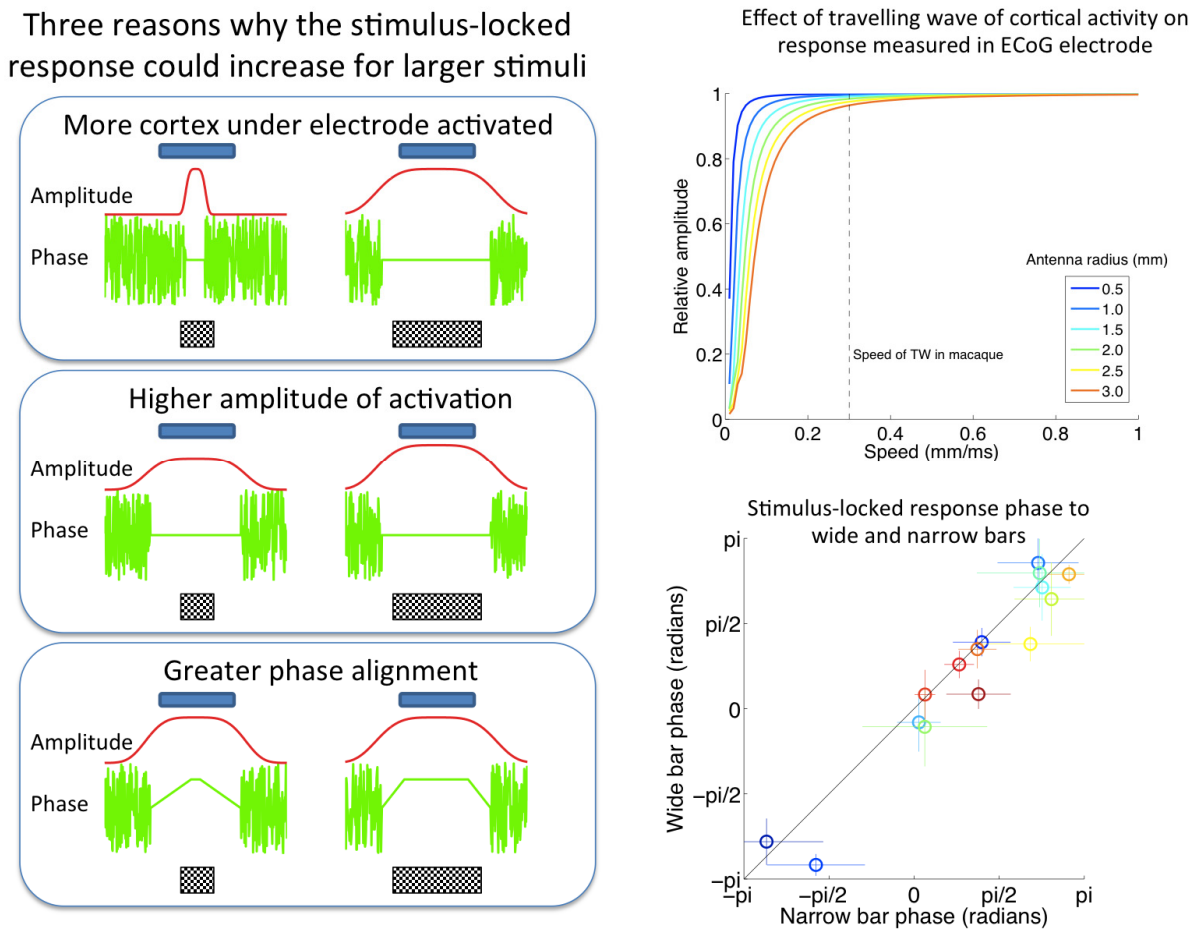

Figure S6. Alternative Models of Cortical Responses to Account for the Larger Stimulus-Locked Response to Wide Bars Compared to Narrow Bars

(Left) The three panels illustrate three response models. Each panel represents the response to a narrow (left) or wide (right) contrast stimulus. In each case the signal amplitude measured by the electrode is greater for the wide bar than the narrow bar (not shown). The blue trace at the top indicates the position and size of the electrode. The red trace shows the amplitude of the mean electrical field potential across cortical space. The green trace shows the relative phase of this signal. The top panel describes the original model in the paper (Figure 6). In this model the steady-state neural signal under the electrode is synchronous at a single amplitude over a spatial extent of cortex that matches the stimulus width. Outside of this range, the amplitude of the stimulus is mean zero and the phase is random. As the stimulus width changes from narrow to wide, an increasing amount of cortex responds. The spatial extent of the response is within the field picked up by the ECoG electrode, and thus the amplitude of the signal in the electrode increases. Hence, in this model, additivity of spatial summation arises because the stimulus-locked signal spreads over larger parts of cortex. The middle panel is an alternative model. In this case, the spatial extent of the stimulus-locked signal is similar for both the narrow and wide bars. The difference in the neural response is the amplitude. On this model, the linearity arises because the response amplitude across a fixed cortical region, say a column,

increases with bar width. Both of these models differ from the observed BOLD response: in each of these models, the neural response summed over a few millimeters of cortex is greater for the wider stimulus (either because of wider spread or higher amplitude), whereas the BOLD signal (and the broadband signal) are similar for narrow and wide stimuli. The third panel shows a model based on the notion of travelling waves of activity on the cortical surface. The spatial extent of cortex excited by the two bar widths is similar, as is the amplitude of the cortical response. The difference is that the narrow bar evokes a response in the central region that spreads laterally. This is indicated by the change in the phase of the neural response from the peak in the middle, falling off on each side. The wide bar evokes a coherent response over a larger amount of cortex, with the traveling wave arising at the edge. According to this model the ECoG amplitude to the wide bar is larger than the narrow bar because of the difference in the phase coherence. The signals add in the wide bar case, but the narrow bar case has the neural signals in different phases that may even combine destructively. In this model, the increase in signal measured by the electrode is explained by the increase in phase coherence rather than more cortical activation.

(Upper right) Simulation of the effect of a traveling wave of cortical activity on the signal amplitude summed by an electrode. The simulation assumes a signal of unit amplitude with phase 0 at the center of the electrode's antenna function, and a lag at other locations that is proportional to the distance, with rates of proportionality ranging from 0.01 mm/ms to 1 mm/ms. The speed of traveling waves reported in the macaque literature is indicated by the black dashed line (0.3 mm / ms) [1]. To compute the aggregate signal amplitude, lags were converted from units of time to units of phase assuming a period of 1/15 second, matched to the time between contrast reversals in our experiments. Several antenna radii were modeled ranging from 0.5 mm to 3.0 mm. The drop in signal amplitude as measured by the electrode is minor at all antenna radii and at all speeds of traveling waves that are close to the measured values in the literature. Only for travelling wave speeds that are much slower than reported is there a substantial signal loss.

(Lower right) The traveling wave hypothesis, as indicated by the lower panel on the left, predicts that the phase of the response measured by the electrode will be delayed for a narrow stimulus compared to a wide stimulus. The scatterplot on the lower right is a summary of data that test this hypothesis. Each circle indicates phase data for one electrode. The phase was computed from the stimulus positions in the bar experiments corresponding to the peak amplitude of each cardinal sweep of the bar (4 sweeps per experiment, 2 or 3 experiments per condition, yielding 8 or 12 measurements per electrode per stimulus type). The mean and standard deviation of the phase (computed in complex coordinates) are plotted for each of the 15 channels (see table 2). The plot shows that (1) phases differ systematically between electrodes, (2) the phases are correlated for the two stimulus types, and (3) on average there is a slight delay for the narrow bars, as predicted by the traveling wave. The delay is a median of 0.13 radians, or 1.4 ms given contrast reversals at 15 times per second (period of 67 ms). This phase delay is consistent with the simulations shown in the upper right and corresponds to an amplitude decrease of less than 1%. Hence the phase data are consistent with the traveling wave hypothesis, but the size of the effect does not explain a stimulus locked amplitude reduction of 50% for small bars compared to large bars (Figure 2d).

Table S1. Summary of Electrodes in Four ECoG Subjects, Related to Figure 2

Subject	Number of Electrodes	V1/V2/V3	AB PRF VE>30%	SL PRF VE>30%	Intersection of columns 3,4,5	AB cross-validated VE>20%	SL cross-validated VE>20%
1	112	9	16	12	8	14	12
2	76	6	6	6	5	6	5
3	78	2	5	4	2	4	3
4	118	34	31	NA	21	34	NA

Column 1 is the subject number. Column 2 is the total number of electrodes recorded from that subject. Column 3 is the number of electrodes within visual field maps V1, V2, or V3. Columns 4 and 5 are the number of electrodes for which the variance explained by the CSS pRF model exceeded 30% for the asynchronous broadband ("AB") time series and stimulus locked ("SL") time series, respectively. Column 6 is the intersection of the previous 3 columns. The 15 electrodes in the first three rows of this column (subjects 1, 2, and 3) are the 15 channels used for several plots and calculations, including the insets in Figure 2c and 2d, the pRF center and exponent plots in Figure 3, and the pRF size histogram in figure S3. Column 7 is the number of channels for which the cross-validated variance explained from either the linear or the compressive AB pRF model exceeded 20%. The channels in this column are plotted in Figure 4a. Column 8 is the number of channels for which the cross-validated variance explained from either the linear or the compressive SL pRF model exceeded 20%. The channels in this column are plotted in Figure 4b. For S4, columns 5 and 8 are not applicable because this subject did not have flickering stimuli, and therefore also did not have an associated stimulus-locked time series.

Table S2. PRF Size and Exponent for 15 Electrodes in Subjects 1, 2, and 3, Related to Figure 3

Subject	Channel	PRF Exponent (25^{th}|50^{th}|75^{th} percentile)		PRF Size (25^{th}|50^{th}|75^{th} percentile)	
		AB	SL	AB	SL
3	54	0.09|0.11|0.14	0.92|1.25|3.30	1.19|1.38|1.55	0.12|0.77|1.00
3	53	0.22|0.28|0.35	1.38|1.47|1.61	0.96|1.09|1.22	1.00|1.09|1.18
2	70	0.03|0.03|0.05	1.02|1.11|1.18	2.66|2.93|3.45	1.61|1.75|1.88
2	69	0.10|0.33|0.46	0.50|0.61|0.76	1.91|2.19|2.40	1.89|2.02|2.14
2	68	0.26|0.32|0.41	0.14|0.40|0.68	1.20|1.35|1.51	1.13|1.43|1.87
2	66	0.34|0.42|0.51	1.31|1.50|1.72	2.05|2.29|2.64	2.80|3.42|3.80
2	65	0.17|0.21|0.27	0.70|0.80|0.90	0.75|1.01|1.20	1.55|1.78|2.01
1	104	0.17|0.21|0.28	0.87|0.99|1.12	0.74|0.81|0.89	0.55|0.65|0.75
1	102	0.13|0.26|0.41	0.57|0.74|0.94	1.83|2.77|4.00	4.68|6.12|9.02
1	70	0.04|0.07|0.11	0.38|0.48|0.59	0.23|0.33|0.47	1.25|1.68|1.99
1	69	0.21|0.97|1.15	0.08|0.12|0.17	0.03|0.06|0.33	1.89|2.16|2.48
1	68	0.46|0.78|1.00	0.13|0.39|0.60	0.05|0.45|0.80	2.31|2.60|2.91
1	67	0.19|0.33|1.00	1.25|1.46|1.66	0.04|0.16|0.31	1.49|1.64|1.83
1	66	0.18|0.53|0.98	0.97|1.15|1.47	0.03|0.04|0.29	1.88|2.54|2.83
1	50	0.15|0.18|0.26	0.77|1.00|1.23	0.81|0.93|1.02	0.92|1.29|1.82

The 15 electrodes correspond to those in column 6 of Table S1 for subjects 1, 2 and 3. The pRF exponent and size values are reported as the 25^{th}, 50^{th}, and 75^{th} percentiles based on 200 bootstrapped model solutions for each channel, for both the asynchronous broadband ("AB") time series and the stimulus locked ("SL") time series. For each subject and model solution, there were 288 time points (3 bar widths and 96 stimulus positions, including blanks), and the bootstrapping was done by randomly sampling with replacement 288 times from these 288 time points.

Supplemental Experimental Procedures

Participants

Participants included four patient volunteers (2 male, 2 female; ages 41-57; 'S1-S4'). Subdural electrodes were implanted for the purpose of pre-surgical evaluation of the source of epileptic seizures. The seizure sources were not in occipital cortex in any of the participants. ECoG recordings took place in the hospital room in the week prior to surgery. Functional MRI experiments were performed on the same participants prior to electrode implantation to identify visual field maps. Three additional participants took part in functional MRI experiments (all male, ages 25-39; 'S5-S7') to assess properties of population Receptive Fields. Informed written consent was obtained from all participants.

Electrode Localization

Electrodes were implanted as either strips or grids (AdTech Medical Instrument Corp). Each electrode was 2.3-mm in diameter (exposed recording area) with center-to-center spacing of 5-10 mm between adjacent electrodes. Positions of the electrodes were identified on post-operative computed tomography (CT) images. These images were then aligned with preoperative anatomical MRIs. A procedure was used to compensate for discrepancies between the two types of brain images caused by shifts in brain structure from electrode implantation [2].

Electrophysiological Recording and Analysis

We recorded signals at 3052 Hz through a 128-channel recording system made by Tucker Davis Technologies (http://www.tdt.com/). We removed channels that had shown any epileptic activity, as determined by the patient's neurologist (JP). Off-line, data were notch filtered to remove line noise and re-referenced to the common average.

Stimuli for ECoG Experiments

Display. ECoG experiments were conducted in the subject's hospital room using a 13-inch MacBook Pro for stimulus presentation, placed as close as possible to the subject (range: 47 cm – 61 cm), with the center of the screen at eye level. All stimuli were confined to a circular aperture whose diameter was equal to the screen height, corresponding to a visual angle of 19.2 – 25.2 deg. The display had a resolution of 1440 x 900 pixels and a nominal refresh rate of 60 Hz. The refresh rate was measured by the Psychtoolbox function 'FrameRate'. The frequency of the square-wave patterns (see below) was adjusted slightly to be an integer multiple of the measured refresh rate (7.466 Hz rather than 7.5 Hz). Display luminance was measured with a Minolta Color Meter II in the patient rooms to quantify image contrast. Minimum and maximum luminance were approximately 24.6 and 203 cd/m^2 for S2, S3, and S1, and 2.4 and 24.7 cd/m^2 for S4, who requested reduced screen and room illumination for comfort.

Bar stimuli. For S1, S2, and S3, bar experiments were similar to those used previously for fMRI experiments [3-5]. A contrast pattern was viewed through a bar aperture that swept across the visual field in 12 1-second steps. There were 8 sweeps across the visual field, including 4 cardinal directions (left to right, right to left, top to bottom, and bottom to top)

interspersed with four diagonals (see Figure 2 for the sequence). The cardinal sweeps consisted of 12 discrete steps whereas the diagonals sweeps consisted of 6 steps (from the screen corner to the screen middle) followed by a 6-second blank (zero-contrast, mean luminance); the blanks help to estimate the baseline response level. For each of these three participants, there were 6 bar experiments comprised by 2 repetitions each of 3 bar widths (1/16, 1/8, and 1/4 the maximum bar height).

For S2 and S3, the contrast of the checkerboard pattern within the moving bars was 78%, the maximum afforded by the display given the ambient illumination in the hospital room. For S1 and S4, the contrast was reduced to 10% and 8%, respectively, to avoid the possibility of saturation in the ECoG responses.

For S4, the design of the bar experiment differed in several important ways. First, the stimuli were presented in random order rather than sweeps across the visual field. Second, stimuli with the 3 bar widths were randomly interspersed rather than tested in separate experiments. Third, there were no blank periods. Fourth, the carrier pattern did not flicker; instead, the stimulus was shown for 100 ms without flicker, with 500 ms interstimulus intervals (400 ms blank between successive stimuli). For each bar aperture, there were two possible carrier patterns (one checkerboard pattern and its contrast-reversed pattern). Additionally, there were 5 full-field circular apertures with various contrasts (see Figure 5), each shown with one of two contrast patterns. Hence a single experiment included 202 events: (48 bar locations * 3 bar widths + 5 full field patterns) * 2 contrast patterns. The experiment was repeated 3 times for this subject.

Large field on-off stimuli. Large field on-off stimuli consisted of a circular aperture (largest circle that completely fit within the display) and a contrast-reversing dartboard pattern (7.5 Hz square wave). Experiments consisted of four 6-s 'on' periods alternated with four 6-s 'off' periods. During the 'off' periods the screen was blank (mean luminance of the contrast pattern) except for a fixation dot.

Fixation task. During bar experiments and 'on-off' experiments, participants viewed a small central fixation dot, which alternated between red and green at random intervals (average once per 3 s). Participants pressed a button on an external number pad to indicate a change in fixation color. The purpose of the fixation task was to ensure central fixation. All participants responded to the fixation color changes with high accuracy.

Visual stimuli were generated on a Macintosh MacBook Pro in the MATLAB programming environment using in-house software, made freely available (http://vistalab.stanford.edu/software/). The software tools are built on functions from the PsychToolbox [6, 7].

Stimuli for fMRI Experiments

Display. Stimuli were presented using a Samsung SyncMaster 305T LCD monitor positioned at the head of the scanner bed. Subjects viewed the monitor via a mirror mounted on the RF coil. The monitor operated at a resolution of 1280 x 800 at 60 Hz, and the luminance response of the monitor was linearized using a lookup table based on spectrophotometer measurements. The minimum and maximum luminance was 1.4 cd/m^2 and 121 cd/m^2,

respectively. Stimuli subtended 12.5–12.8° of visual angle. A button box recorded behavioral responses.

Bar stimuli. The bar stimuli used in fMRI experiments with control subjects were the same as those used in ECoG experiments except for two differences: the duration of each aperture position was 1.5 s rather than 1 s; the number of discrete steps in one sweep of the visual field was 16 rather than 12; the contrast pattern within the aperture drifted rather than flickered (2 Hz temporal frequency) (see [3] and [4]). For each subject, there were 9 bar experiments – 3 with each of three bar widths. Bar stimuli for ECoG subjects were used only to identify visual field maps, not to assess spatial summation. Hence only one bar width was used – 1/8 the length of the bar – the same as the middle width used in control subject fMRI experiments and in ECoG experiments).

Broadband and Stimulus-Locked EcoG Responses

The time series of the broadband and stimulus-locked responses to bar stimuli were constructed by short-time Fourier analysis. The window for Fourier analysis was the duration that a stimulus aperture remained in a position (1 second for participants S2, S1, and S3, bar; 0.5 s for S4, who had an event-related design rather than sweeps across the visual field). The time series from the one second window was multiplied by a Hann window (raised cosine) to reduce edge artifacts.

For the broadband data, a line was fit in log-log space to the signal power (squared amplitude) of Fourier components from 8 Hz to 150 Hz, excluding values within 2 Hz of even harmonics of the stimulus frequency (15, 30, 45, 60, 75, 90, 115, 120, 135, and 150 Hz) (Figure 1d). The slope of the line was forced to be the same for all stimulus positions for a given electrode. The height of the line at 15 Hz was taken as the broadband signal for that time point. The stimulus-locked signal was defined as the amplitude at 15 Hz, after subtracting the broadband fit. Calculations were also run on the stimulus locked time series omitting the subtraction of the broadband fit; the pattern of effects is unchanged, with only a small change in the parameter values.

The approximately linear relationship between power and frequency holds in our data between 10 Hz and 150 Hz. It is less reliable below 10 Hz, due to rhythmic processes in the alpha band (observed in some electrodes and some conditions).

Spectral power was used to measure the broadband response. We use power rather than amplitude because when the temporal frequency phases are random signal superposition is additive with respect to power. Specifically, if the phases are random the sum of the power spectrum of signal X and the power spectrum of signal Y is on average the power spectrum of signals X + Y. Amplitude was used as the dependent measure for the stimulus-locked signal because the phase of the response at stimulus harmonics (e.g., 15 Hz) were roughly constant across trials; if the phase is constant, amplitude rather than power is additive (see Figure S5).

PRF Models

The CSS model fitting procedure is described in detail elsewhere [8]. An outline of the procedure and a few details that differ from prior work are described in Results.

The CSS model was fit to each voxel time series (fMRI) or broadband or stimulus-locked time series (ECoG) by minimizing the difference between the predicted response and the observed response, according to a least squares metric using nonlinear optimization (MATLAB Optimization Toolbox). Before fitting the model, data were preprocessed and averaged across repeated experiments.

Models were fit in two different ways. To derive model parameters, data from experiments with all 3 bar widths were concatenated, and the best fitting parameters were found. To quantify accuracy, parameters were derived from experiments with two of three bar widths (test data), and then applied to the experiments with the third bar width (test data). The accuracy metric was the coefficient of determination,

$$R^2 = 100 \times \frac{1 - \sum(model - data)^2}{\sum(data)^2}$$

The model was seeded with a Gaussian centered at the image center, *sigma* equal to the maximum stimulus extent, and $n = 1$. To reduce the chance of finding a local minimum, the model was solved stepwise. In the first iteration, n was fixed at 1 and the x,y, sigma, and gain parameters were optimized. In the second iteration, n was allowed to vary. For fMRI data, the model convolved the response output with a hemodynamic response function based on a difference of two gamma functions [9].

To compare the accuracy of CSS model fits with that of the linear model, we performed a fit with the exponent n fixed at 1. This yields a linear solution whose cross-validation accuracy was compared to the CSS solution, with n free to vary (Figure S4).

Simulation of the ECoG Temporal Responses

We implemented software to simulate the main features of the ECoG responses. The principles and simulations are described in Results. The full MATLAB code implementing the simulation, including examples and the code needed to reproduce the simulation in Results, is available at [10].

Channel Selection

Several analyses were conducted across channels, necessitating criteria for the selection of channels. Channel selection is described below and summarized in Table S2.

Three criteria were used to select channels for calculating the mean ECoG responses to 'on-off' stimuli (Figure 1 and related results), the mean peak responses during the moving bar experiments (Figure 2, insets), the pRF center positions and sizes (Figure 3b and related results), and the phase of the stimulus-locked response during moving bar experiments (Figure S6, lower right). The first criterion was that the cortical location was V1, V2 or V3. For several reasons, electrodes within any of these three field maps were grouped for analysis. These field maps produce robust responses to the simple contrast patterns used in our experiments. Also, not having enough electrodes to sample each map in each subject in similar receptive field locations, we thought it best to combine data across channels; V1, V2, and V3 share many qualitative response properties. Finally, because several of the electrodes were on the borders of visual fields (all the electrodes are on gyri), we frequently could not distinguish V1 from V2 or V2 from V3.

The second criterion was that the variance explained from pRF models exceeded 30% for both broadband and stimulus-locked responses. The third criterion was that the stimuli

were presented to the subject as periodic contrast reversals (S1, S2, S3) rather than as a static pattern (S4).

This selection yielded 15 channels (8 from S1, 5 from S2, and 2 from S3). To summarize the compressive exponent from the CSS model (Figure 3c), the same 15 channels were used.

In a separate calculation, data from 21 channels in S4 were used to calculate the broadband exponent but not the stimulus-locked exponent, as experiments for S4 did not have periodic flicker, and hence no narrow-band stimulus-locked response (SSVEP). Including these 21 channels did not change the pattern of results, as the mean exponent did not differ among the four subjects (one way ANOVA, $F = 0.29$; $P = 0.83$).

To choose channels for calculating accuracy of the CSS model, both linear and non-linear models were first fit to all channels using all data from experiments with 3 bar aperture widths for all 4 subjects. Channels with at least 20% variance explained from either the linear model or the CSS model were selected for further analysis in which accuracy was calculated via leave-one-out cross-validation (Figure 4). These selection criteria were determined separately for the broadband and the stimulus-locked responses.

Anatomical and Functional MRI

MRI sessions were conducted to localize visual field maps and to study properties of the BOLD response in visual cortex. For patient volunteers, the MRI session took place prior to electrode implantation. Methods for anatomical and functional MRI followed those reported in previous work [4], with a few minor differences. We summarize the main procedures here and those details that differ from prior work.

T1-weighted anatomical scans (3D SPGR) of the whole brain were acquired at 1-mm resolution (ECoG subjects) or 0.7 mm resolution (control subjects). The T1-weighted images were segmented into gray/white voxels using FreeSurfer's autosegmentation algorithm (http://surfer.nmr.mgh.harvard.edu/)[11], followed by hand-editing in itkGRAY [12] to correct errors. In addition, a separate T1-weighted anatomical scan was acquired in conjunction with fMRI scans that matched the slice prescription of the functional scans. This 'inplane' anatomical scan was used to co-register the functional images with the whole-brain T1 image. Functional MRI scans were acquired as echo planar images either with a spiral trajectory (Lucas Center, Stanford University) or with a rectilinear trajectory (CNI, Stanford University). In each case, the functional images were undistorted using in-house software [8].

Visual field maps were identified based on fMRI data as described in previous work [4].

Data and Code Sharing

Sample data sets and the complete set of MATLAB code needed to run the ECoG simulations in the manuscript and to produce several of the data figures are publicly available [10]. The goal is to ensure that the computational methods are reproducible by other researchers [13].

Supplemental References

1. Nauhaus, I., Busse, L., Ringach, D.L., and Carandini, M. (2012). Robustness of traveling waves in ongoing activity of visual cortex. J Neurosci *32*, 3088-3094.
2. Hermes, D., Miller, K.J., Noordmans, H.J., Vansteensel, M.J., and Ramsey, N.F. (2010). Automated electrocorticographic electrode localization on individually rendered brain surfaces. J Neurosci Methods *185*, 293-298.
3. Dumoulin, S.O., and Wandell, B.A. (2008). Population receptive field estimates in human visual cortex. Neuroimage *39*, 647-660.
4. Winawer, J., Horiguchi, H., Sayres, R.A., Amano, K., and Wandell, B.A. (2010). Mapping hV4 and ventral occipital cortex: the venous eclipse. J Vis *10*, 1.
5. Amano, K., Wandell, B.A., and Dumoulin, S.O. (2009). Visual field maps, population receptive field sizes, and visual field coverage in the human MT+ complex. J Neurophysiol *102*, 2704-2718.
6. Pelli, D.G. (1997). The VideoToolbox software for visual psychophysics: transforming numbers into movies. Spat Vis *10*, 437-442.
7. Brainard, D.H. (1997). The Psychophysics Toolbox. Spat Vis *10*, 433-436.
8. Kay, K.N., Winawer, J., Mezer, A., and Wandell, B.A. (2013). Compressive spatial summation in human visual cortex. J Neurophysiol. Published online April 24, 2013. 10.1152/jn.00105.2013
9. Friston, K.J., Fletcher, P., Josephs, O., Holmes, A., Rugg, M.D., and Turner, R. (1998). Event-related fMRI: characterizing differential responses. Neuroimage *7*, 30-40.
10. Winawer, J., Kay, K., Foster, B.L., Rauschecker, A.M., Parvizi, J., and Wandell, B.A. (2013). Stanford Digital Repository: Code and data supplement for "Asynchronous broadband signals are the principal source of the BOLD response in human visual cortex". http://purl.stanford.edu/hj582pj3902.
11. Dale, A.M., Fischl, B., and Sereno, M.I. (1999). Cortical surface-based analysis. I. Segmentation and surface reconstruction. NeuroImage *9*, 179-194.
12. Yushkevich, P.A., Piven, J., Hazlett, H.C., Smith, R.G., Ho, S., Gee, J.C., and Gerig, G. (2006). User-guided 3D active contour segmentation of anatomical structures: Significantly improved efficiency and reliability. Neuroimage *31*, 1116-1128.
13. Gavish, M., and Donoho, D. (2012). Three dream applications of verifiable computational results. Comput Sci Eng *14*, 26.